

## Atomic Layer Deposition of LiOH and Li<sub>2</sub>CO<sub>3</sub> Using Lithium t-butoxide as the Lithium Source

A.S. Cavanagh<sup>a,b</sup>, Y. Lee<sup>c</sup>, B. Yoon<sup>c</sup> and S.M. George<sup>c,d</sup>

<sup>a</sup> Department of Physics, University of Colorado, Boulder, Colorado 80309, U.S.A.

<sup>b</sup> DARPA Center for Integrated Micro/Nano-Electromechanical Transducers (iMINT),  
University of Colorado, Boulder, Colorado 80309, U.S.A.

<sup>c</sup> Department of Chemistry and Biochemistry, University of Colorado, Boulder, Colorado  
80309, U.S.A.

<sup>d</sup> Department of Chemical and Biological Engineering, University of Colorado, Boulder,  
Colorado 80309, U.S.A.

Atomic layer deposition (ALD) was utilized to grow LiOH and Li<sub>2</sub>CO<sub>3</sub> films using lithium tert-butoxide, H<sub>2</sub>O and CO<sub>2</sub>. Film growth was monitored with a quartz crystal microbalance at 225°C. LiOH ALD had a growth rate of 12.7 ng·cm<sup>-2</sup>·cycle<sup>-1</sup> before displaying evidence for hygroscopic behavior. Li<sub>2</sub>CO<sub>3</sub> ALD had a growth rate of 17.1 ng·cm<sup>-2</sup>·cycle<sup>-1</sup>. The film identities were confirmed using Fourier transform infrared and X-ray photoelectron spectroscopies. Lithium-containing films are present in the solid-electrolyte interphase (SEI) on graphite anodes of Li-ion batteries. The ALD of an artificial SEI layer may limit lithium loss and improve the capacity stability during charge-discharge cycles.

### Introduction

Graphite is a common anode material in Li ion batteries (LIBs) (1-2). Decomposition of electrolyte during charge-discharge cycling leads to the growth of a solid-electrolyte interphase (SEI) layer on the graphite electrode (3-4). The SEI layer restricts lithium diffusion and electron conductivity to the graphite electrode (5-6). Lithium bound in the SEI layer also removes lithium from charge transport and lowers the battery capacity (5-6). The composition of the SEI layer includes various lithium compounds such as Li<sub>2</sub>CO<sub>3</sub>, Li<sub>2</sub>O, LiOH, LiF and ROLi (5, 7). The deposition of an artificial SEI layer on the graphite anode may be useful to prevent lithium loss and limit capacity reduction during charge-discharge cycling (8).

In this paper, two possible artificial SEI materials, LiOH and Li<sub>2</sub>CO<sub>3</sub>, are grown with atomic layer deposition (ALD) techniques using lithium tert-butoxide (LTB), H<sub>2</sub>O and CO<sub>2</sub> as the reactants. ALD is a thin film deposition technique based on sequential, self-limiting surface reactions (9-10). ALD can deposit atomic layer controlled and conformal films on very high aspect substrates (11). In addition, ALD can be employed to deposit films on particles and on porous substrates (12). ALD could be used to deposit artificial SEI layers either on graphite particles used to make the anode or on the porous anode formed from graphite particles.

## Experimental

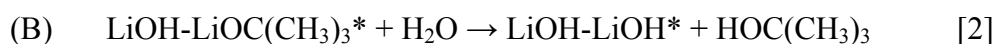
The LiOH and Li<sub>2</sub>CO<sub>3</sub> films were grown in a viscous flow ALD reactor that has been described elsewhere (13). The LTB source was held at 165 °C and the reactor was maintained at 225 °C. The reaction was monitored *in situ* with a Maxtek, Inc. BSH-150 quartz crystal microbalance (QCM). LiOH ALD films were grown by sequential exposure to LTB (98+%, Strem Chemicals) and H<sub>2</sub>O (HPLC grade, Honeywell). Li<sub>2</sub>CO<sub>3</sub> ALD is based on a ternary ABC reaction sequence. Li<sub>2</sub>CO<sub>3</sub> ALD films were grown by sequential exposure to LTB, H<sub>2</sub>O and CO<sub>2</sub> (bone dry, Matheson Trigas). The LTB dose was 3 s with a partial pressure of 4.0 Pa. The H<sub>2</sub>O dose was 1 s with a partial pressure of 33.3 Pa. The CO<sub>2</sub> dose was 1 s with a partial pressure of 66.7 Pa. The purge times after the reactant exposures were 60 s.

Fourier transform infrared spectroscopy (FTIR) was used to determine the film identity. LiOH and Li<sub>2</sub>CO<sub>3</sub> ALD films were grown on KBr slides (International Crystal Laboratories) and characterized *ex situ* with a Nicolet Avatar 360 FTIR. Due to the instability of LiOH in air, LiOH films were also grown in an ALD reactor equipped with *in situ* FTIR analysis that has been described elsewhere (14). The *in situ* FTIR studies were performed with a Nicolet Nexus 870 FTIR spectrometer.

The LiOH and Li<sub>2</sub>CO<sub>3</sub> films were also characterized *ex situ* with X-ray photoelectron spectroscopy (XPS). Measurements were performed with a Perkin-Elmer 5600 XPS using a monochromatic Al K $\alpha$  source (1486.6 eV). The base pressure in the vacuum chamber during XPS analysis was  $1.3 \times 10^{-8}$  Pa. A constant analyzer energy mode was employed at a pass energy of 58.7 eV with a step size of 0.25 eV.

## Results and Discussion

LiOH ALD film growth was monitored using the QCM. The overall binary reaction is  $\text{LiOC}(\text{CH}_3)_3 + \text{H}_2\text{O} \rightarrow \text{LiOH} + \text{HOC}(\text{CH}_3)_3$ . The AB binary reaction sequence during LiOH ALD is proposed to be:



where an asterisk is used to denote surface species. LiOH-LiOC(CH<sub>3</sub>)<sub>3</sub>\* is postulated to be a molecularly adsorbed species that reacts with H<sub>2</sub>O to form LiOH.

The first 3 cycles during LiOH ALD are shown in Fig. 1a. During the first 10 ALD cycles, the mass gain during the LTB exposure was  $\Delta m_A = 30.1 \text{ ng}\cdot\text{cm}^{-2}\cdot\text{cycle}^{-1}$  and the mass loss during the H<sub>2</sub>O exposure was  $\Delta m_B = -18.6 \text{ ng}\cdot\text{cm}^{-2}\cdot\text{cycle}^{-1}$ . The  $\Delta m_A/\Delta m_B$  ratio was -1.62. This ratio is close to the predicted ratio of -1.43 based on Eqns. 1 and 2. After the first 10 LiOH ALD cycles, the mass changes evolve and display a much different behavior. Figure 1b shows the QCM results during cycles 198-200.

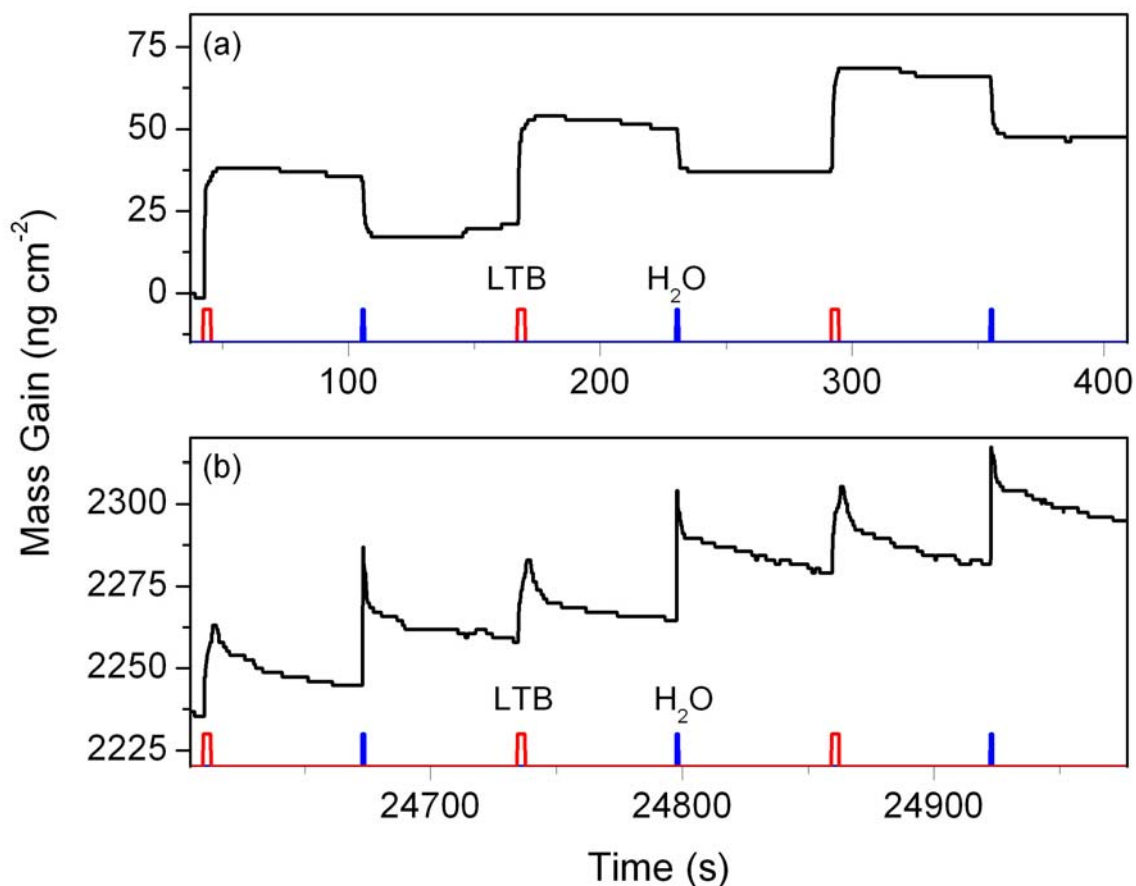
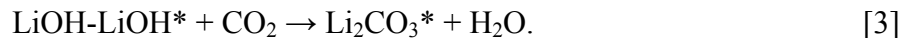


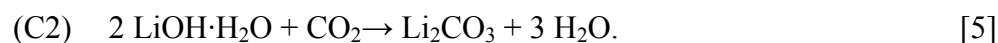
Figure 1. Mass gain during LiOH ALD using LTB and H<sub>2</sub>O at 225°C for (a) cycles 1-3 and (b) cycles 198-200.

LiOH is hygroscopic and can easily adsorb H<sub>2</sub>O and form a hydrate (15). The hygroscopicity is reversible and H<sub>2</sub>O can desorb from the LiOH-hydrate during the purge times (15). This H<sub>2</sub>O desorption leads to the mass decays observed after both the LTB and H<sub>2</sub>O exposures in Fig. 1b. To confirm the presence of a LiOH-hydrate, films grown using 200 AB cycles were subjected to an extended N<sub>2</sub> purge at 225°C. The LiOH film lost ~32% of its mass in 2 hours before reaching a stable value. This mass loss is attributed to H<sub>2</sub>O desorption from the LiOH-hydrate.

Li<sub>2</sub>CO<sub>3</sub> ALD is based on a ternary ABC reaction sequence that utilizes the LTB and H<sub>2</sub>O reactions given in Eqns. 1 and 2. In addition, a third reaction is added where LiOH can react with CO<sub>2</sub> to form Li<sub>2</sub>CO<sub>3</sub> according to (15):



The reaction in Eqn. 3 relies on the presence of H<sub>2</sub>O and has been shown to involve LiOH·H<sub>2</sub>O (lithium hydroxide hydrate) according to (15):



Although H<sub>2</sub>O is required to initiate the reaction, H<sub>2</sub>O products sustain the reaction.

The LiOH film can be easily converted to  $\text{Li}_2\text{CO}_3$  by exposure to  $\text{CO}_2$  (15-16). Figure 2a shows the QCM results when a LiOH film grown using 200 AB cycles is exposed to ABC cycles of LTB,  $\text{H}_2\text{O}$  and  $\text{CO}_2$ . Large mass gains of  $\Delta m_C = 552.9, 224.3, 110.8 \text{ ng}\cdot\text{cm}^{-2}\cdot\text{cycle}^{-1}$  were observed during the first three  $\text{CO}_2$  exposures. The mass gains during the  $\text{CO}_2$  exposures then decreased rapidly and reached a stable mass gain of  $\Delta m_C = 5.3 \text{ ng}\cdot\text{cm}^{-2}$  after 25 cycles.

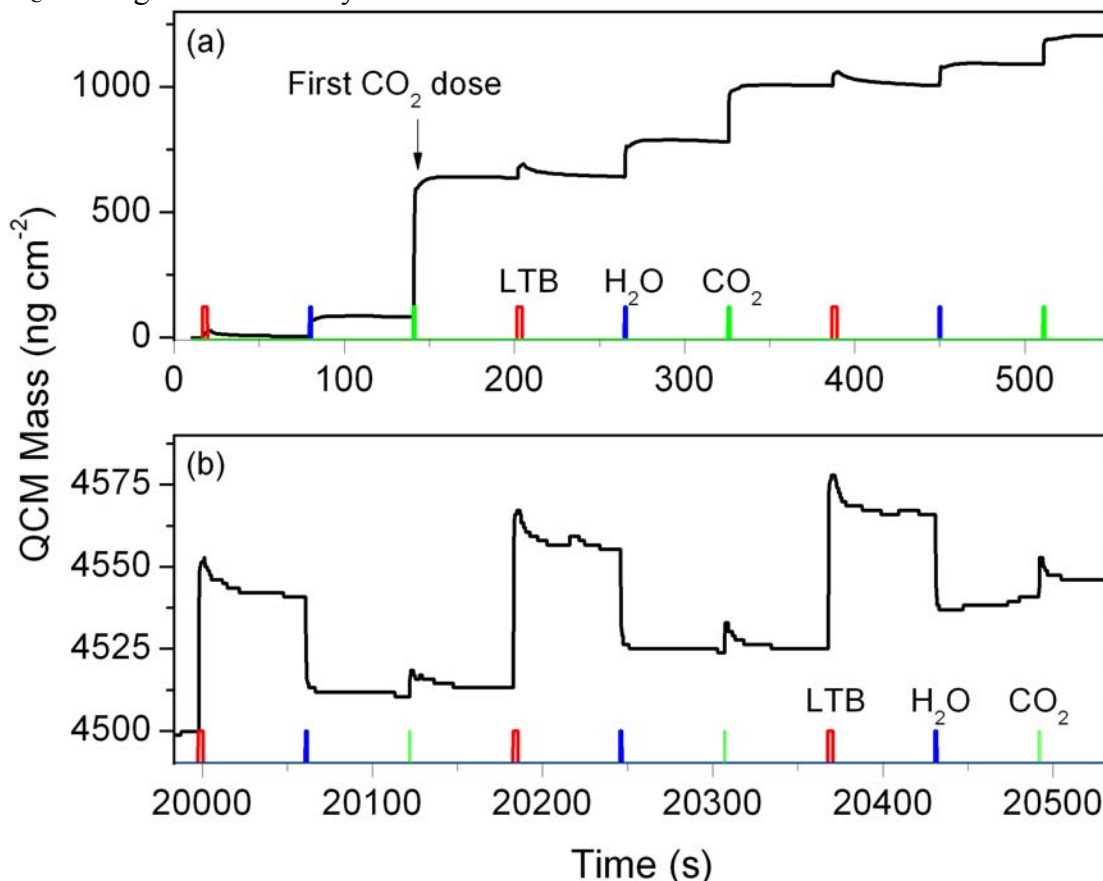


Figure 2. Mass gain during  $\text{Li}_2\text{CO}_3$  ALD using LTB,  $\text{H}_2\text{O}$  and  $\text{CO}_2$  at  $225^\circ\text{C}$  for (a) cycles 1-3 and (b) cycles 198-200.

The large mass gains during the initial  $\text{CO}_2$  exposures are attributed to the conversion of LiOH to  $\text{Li}_2\text{CO}_3$ . The mass of the LiOH film was  $1548.2 \text{ ng}\cdot\text{cm}^{-2}$  after the LiOH films were grown using 200 cycles and stabilized by an extended  $\text{N}_2$  purge. The conversion of this LiOH film to  $\text{Li}_2\text{CO}_3$  by  $\text{CO}_2$  exposures should produce a mass gain of  $863.4 \text{ ng}\cdot\text{cm}^{-2}$ . In close agreement, the total mass gain during the first three  $\text{CO}_2$  exposures was  $888.0 \text{ ng}\cdot\text{cm}^{-2}$ . After approximately 25 cycles of LTB,  $\text{H}_2\text{O}$  and  $\text{CO}_2$ , the  $\text{Li}_2\text{CO}_3$  ALD growth rate stabilized at a mass gain of  $17.1 \text{ ng}\cdot\text{cm}^{-2}\cdot\text{cycle}^{-1}$ . Assuming a  $\text{Li}_2\text{CO}_3$  bulk density of  $2.11 \text{ g}\cdot\text{cm}^{-3}$ , the mass gain of  $17.1 \text{ ng}\cdot\text{cm}^{-2}\cdot\text{cycle}^{-1}$  is equivalent to a  $\text{Li}_2\text{CO}_3$  ALD growth rate of  $0.8 \text{ \AA}\cdot\text{cycle}^{-1}$ .

Figure 2b shows the QCM results during cycles 198-200. The mass gain during the LTB exposure was  $\Delta m_A = 40.6 \text{ ng}\cdot\text{cm}^{-2}$ , the mass loss during the  $\text{H}_2\text{O}$  exposure was  $\Delta m_B = -27.9 \text{ ng}\cdot\text{cm}^{-2}$ , and the mass gain during the  $\text{CO}_2$  exposure was  $\Delta m_C = 5.3 \text{ ng}\cdot\text{cm}^{-2}$ . Figure 3 shows the mass ratios versus the number of ALD cycles. After 25 cycles, the mass ratios are  $\Delta m_A/\Delta m_B = -1.49$ ,  $\Delta m_C/\Delta m_A = 0.13$  and  $\Delta m_C/\Delta m_B = -0.19$ . In comparison, the

mass ratios calculated from Eqns. 1-3 are  $\Delta m_A/\Delta m_B = -1.43$ ,  $\Delta m_C/\Delta m_A = 0.16$  and  $\Delta m_C/\Delta m_B = -0.23$ . These predicted ratios are given by the solid lines in Fig. 3. The agreement between the predicted mass ratios and the measured mass ratios is excellent and supports the reaction mechanism proposed in Eqns. 1-3.

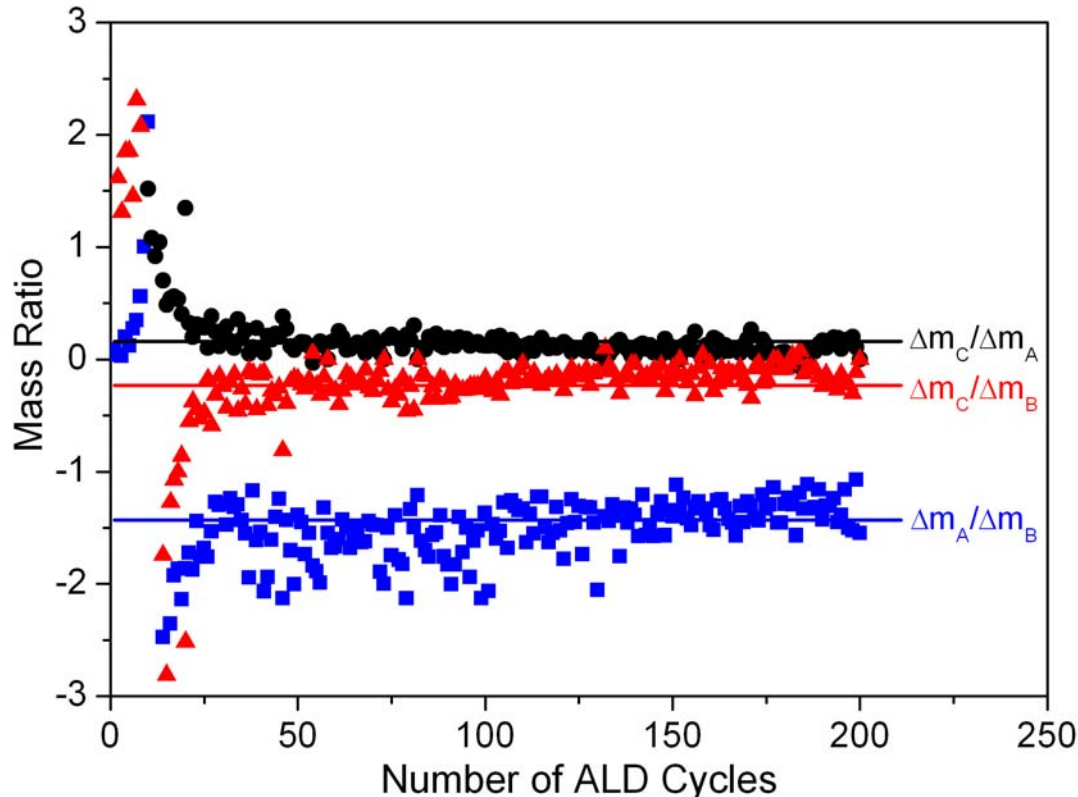


Figure 3. Mass ratios of the mass changes during the LTB (A), H<sub>2</sub>O (B) and CO<sub>2</sub> (C) exposures versus the number of ALD cycles. The solid lines indicate the predicted values expected from Eqns. 1-3.

LiOH and Li<sub>2</sub>CO<sub>3</sub> ALD films were also grown on KBr slides and characterized using *ex situ* FTIR. Removal of the LiOH film from the reactor resulted in the conversion of LiOH to Li<sub>2</sub>CO<sub>3</sub>. Li<sub>2</sub>CO<sub>3</sub> was observed after both LiOH and Li<sub>2</sub>CO<sub>3</sub> ALD. The main absorption bands of Li<sub>2</sub>CO<sub>3</sub> were observed at 1475 cm<sup>-1</sup> and 1429 cm<sup>-1</sup> for antisymmetric C-O stretching vibrations, 1088 cm<sup>-1</sup> for symmetric C-O stretching vibrations, and 870 cm<sup>-1</sup> for out of plane deformation modes (17). All of these features are from the carbonate CO<sub>3</sub><sup>2-</sup> ion.

Figure 4 shows an *in situ* FTIR spectrum after 100 cycles of LiOH ALD on ZrO<sub>2</sub> nanoparticles at 225°C. After deposition, the LiOH ALD film was maintained in the ALD reactor under vacuum. A sharp absorption peak was observed at 3672 cm<sup>-1</sup> that is consistent with hydroxyl stretching vibrations from unhydrated LiOH (16, 18). The O-H stretching vibration from H<sub>2</sub>O in LiOH·H<sub>2</sub>O is not observed at 3570-3574 cm<sup>-1</sup> (16, 18). The absence of this hydrate feature supports the identification of this film as LiOH.

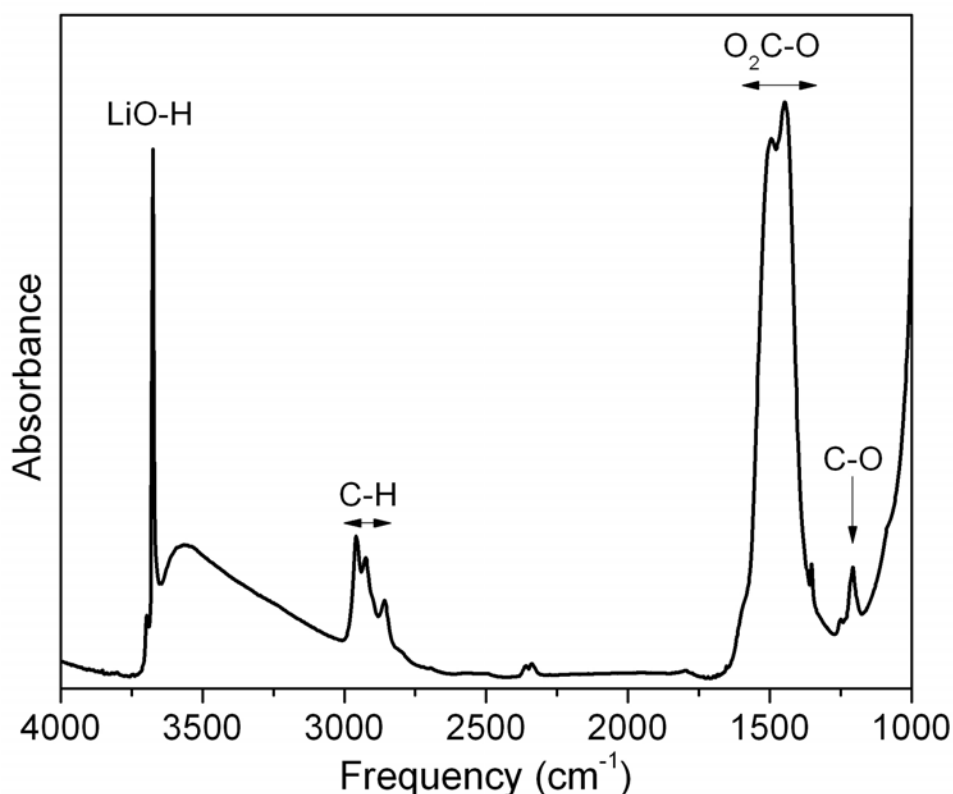


Figure 4. *In situ* FTIR spectrum of a LiOH ALD film grown using 100 cycles of LTB and H<sub>2</sub>O at 225°C. The absorbance from O<sub>2</sub>C-O stretching vibrations indicates the presence of some Li<sub>2</sub>CO<sub>3</sub> from reaction with CO<sub>2</sub>.

There is also a broad absorbance feature from O-H stretching vibrations at 3720-3220 cm<sup>-1</sup> in Fig. 4. This absorbance could be caused by some hydrogen-bonded LiOH hydroxyls or some H<sub>2</sub>O in the LiOH film (16, 18). This absorbance feature also increased with subsequent H<sub>2</sub>O exposure and decreased with purging time after H<sub>2</sub>O exposure. However, the O-H stretching vibration from H<sub>2</sub>O in LiOH·H<sub>2</sub>O was never observed at 3570-3574 cm<sup>-1</sup> after H<sub>2</sub>O exposures to the LiOH ALD film.

The strong absorbances at 1496 and 1450 cm<sup>-1</sup> in Fig. 4 are assigned to antisymmetric C-O stretching vibrations from some Li<sub>2</sub>CO<sub>3</sub> in the LiOH film (16-17). This feature is explained by the facile reaction of LiOH with background CO<sub>2</sub> in the ALD reactor (15-16). In addition, absorbance from C-H stretching vibrations at 3000-2817 cm<sup>-1</sup> and C-O stretching vibrations at 1200 cm<sup>-1</sup> indicates that some unreacted tert-butoxide groups remain in the film.

The LiOH and Li<sub>2</sub>CO<sub>3</sub> films were also characterized *ex situ* with x-ray photoelectron spectroscopy (XPS). After sputtering, the C 1s peak at 289.5 eV was attributed to the formation of Li<sub>2</sub>CO<sub>3</sub>. For the LiOH film, conversion to Li<sub>2</sub>CO<sub>3</sub> occurs upon exposure to CO<sub>2</sub> in air. The Li<sub>2</sub>CO<sub>3</sub> ALD film has a composition of 32.7% lithium, 19.0% carbon and 48.3% oxygen. The uncertainty of these atomic percentages is <2%. In comparison, stoichiometric Li<sub>2</sub>CO<sub>3</sub> has a composition of 33.3% lithium, 16.7% carbon and 50.0% oxygen. This excellent agreement argues that the Li<sub>2</sub>CO<sub>3</sub> ALD film is close to stoichiometric Li<sub>2</sub>CO<sub>3</sub>. The slightly higher levels of carbon and decreased levels of oxygen in the Li<sub>2</sub>CO<sub>3</sub> ALD films may result from some unreacted tert-butoxide groups.

## Conclusions

ALD techniques have been demonstrated for depositing LiOH and Li<sub>2</sub>CO<sub>3</sub> using LTB, H<sub>2</sub>O and CO<sub>2</sub> reactants. The QCM results illustrate the initial growth of LiOH with sequential LTB and H<sub>2</sub>O exposures and reveal the very hygroscopic nature of LiOH. The reaction of LiOH with CO<sub>2</sub> is facile as observed by QCM and FTIR investigations. Li<sub>2</sub>CO<sub>3</sub> ALD growth was also accomplished using sequential LTB, H<sub>2</sub>O and CO<sub>2</sub> exposures. The identity of the Li<sub>2</sub>CO<sub>3</sub> films was confirmed by FTIR and XPS investigations. LiOH and Li<sub>2</sub>CO<sub>3</sub> ALD films may serve as artificial SEI layers to enhance the performance of graphite anodes in LIBs.

## Acknowledgements

This study was supported by the DARPA Center on Nanoscale Science and Technology for Integrated Micro/Nano-Electromechanical Transducers (iMINT) funded by DARPA/MEMS S&T Fundamentals Program (HR0011-06-1-0048). Additional funding was contributed by the National Science Foundation (CHE-0715552). Some of the equipment used in this research was provided by the Air Force Office of Scientific Research.

## References

1. S. Flandrois and B. Simon, *Carbon*, **37**, 165 (1999).
2. J. M. Tarascon and M. Armand, *Nature*, **414**, 359 (2001).
3. D. Aurbach, Y. Eineli, B. Markovsky, A. Zaban, S. Luski, Y. Carmeli and H. Yamin, *J. Electrochem. Soc.*, **142**, 2882 (1995).
4. R. Imhof and P. Novak, *J. Electrochem. Soc.*, **145**, 1081 (1998).
5. E. Peled, D. Golodnitsky and G. Ardel, *J. Electrochem. Soc.*, **144**, L208 (1997).
6. R. Yazami, *Electrochim. Acta* **45**, 87 (1999).
7. M. Dolle, S. Grugeon, B. Beaudoin, L. Dupont and J. M. Tarascon, *J. Power Sources*, **97-8**, 104 (2001).
8. W. S. Kim, K. I. Chung, J. H. Cho, D. W. Park, C. Y. Kim and Y. K. Choi, *J. Ind. Eng. Chem.*, **9**, 699 (2003).
9. S. M. George, *Chem. Rev.*, **110**, 111 (2010).
10. M. Ritala and M. Leskela, *Handbook of Thin Film Materials*, p. 103, Academic, San Diego (2002).
11. J. W. Elam, D. Routkevitch, P. P. Mardilovich and S. M. George, *Chem. Mater.*, **15**, 3507 (2003).
12. J. D. Ferguson, A. W. Weimer and S. M. George, *Thin Solid Films*, **371**, 95 (2000).
13. J. W. Elam, M. D. Groner and S. M. George, *Rev. Sci. Instrum.*, **73**, 2981 (2002).
14. B. Yoon, J. L. O'Patches, D. Seghete, A. S. Cavanagh and S. M. George, *Chem. Vap. Deposition* **15**, 112 (2009).
15. D. D. Williams and R. R. Miller, *Ind. Eng. Chem. Fundam.*, **9**, 454 (1970).
16. N. R. Smyrl, E. L. Fuller and G. L. Powell, *Appl. Spectrosc.*, **37**, 38 (1983).
17. M. H. Brooker and J. B. Bates, *J. Chem. Phys.*, **54**, 4788 (1971).
18. L. H. Jones, *J. Chem. Phys.*, **22**, 217 (1954).